Journal of Engineering Mathematics **23**: 187–202, 1989.

Separated flow past three-dimensional bodies as a singular perturbation problem

P. BASSANINI[1] and A.R. ELCRAT[2]
[1]*Dipartimento di Matematica, Università di Roma I, Città Universitaria, 00185 Roma, Italy*
[2]*Department of Mathematics, Wichita State University, Wichita, Kansas 67208, U.S.A.*

Received 1 February 1988; accepted 26 October 1988

Abstract. This paper proposes a method for computing steady wake flows of an inviscid fluid over a three-dimensional body with polygonal cross-section and arbitrary plan-form. The method is based on the technique of matched asymptotic expansions, assuming a large "aspect ratio". The far-field velocity potential is given essentially by a lifting line and a line source. The near-field, treated as two-dimensional, is solved by a suitable version of Tulin's double spiral vortex model which incorporates a downwash correction and an underpressure in the near-wake. The latter is related to the Reynolds number of the corresponding real flow using recent results by Tulin and Hsu and the authors. Numerical results for a few prototype problems (flat-plate airfoil with separation at both the leading edge and the upper surface, flat-plate wing with full or partial spoiler) are presented. The method can be efficiently implemented on a parallel computer.

1. Introduction

Flows past a three-dimensional body with separation and wakes are of considerable interest and importance in engineering design and analysis. While viscous effects are essentially involved in these phenomena there are many problems in which inviscid models are appropriate since separation occurs at sharp edges and is not sensitive to the Reynolds number. We consider here separated flow past both bluff bodies and lifting surfaces as a singular perturbation problem, the perturbation parameter being related to the "aspect ratio" of the body. The procedure is that of matched asymptotic expansions as has been used earlier by Van Dyke [1] for unseparated flow, Furuya [2] for hydrofoils below a free surface, Sclavounos [3] and Ahmadi and Widnall [4] for unsteady unseparated flows. The inner solution (near-field) is a version of the Tulin double spiral vortex model for two-dimensional wakes, and the outer solution (far-field) is a version of Prandtl's lifting line which includes a line source distribution for a bluff body. The Tulin flows are computed using the efficient algorithm recently introduced by Elcrat and Trefethen [5] for Helmholtz–Kirchhoff flows, and the matching uses expressions for the downwash and circulation distribution which are interpolated by Tchebychev polynomials. The matching is accomplished by an iteration which converges rapidly if an appropriate relaxation parameter is used. Related problems and methods of solution are reviewed in Street's paper [6].

We are considering bodies with polygonal cross-sections and arbitrary planform in a flow which is parallel at infinity. The fluid is inviscid and incompressible, and the density, ϱ_0, and speed at infinity, q_∞, are normalized to one. We choose a coordinate system x_1, x_2, x_3, so that the flow at infinity is in the x_1 direction and the body contains the segment on the x_3 axis between -1 and 1 and has span equal to 2. The geometry is then specified by giving

the polygonal sections as functions of x_3. We denote by $l(x_3)$ a representative dimension of the section which can be used to define the "aspect ratio". For example, if the body is a flat-plate wing, $l(x_3)$ is the chord. We restrict our attention throughout the paper to spanwise symmetric bodies, so that $l(x_3) = l(-x_3)$.

We choose $\varepsilon = l(0)/2$ as our perturbation parameter. We are taking ε small so that the "aspect ratio" is large (for a flat rectangular wing $\varepsilon = (\mathrm{AR})^{-1}$, with aspect ratio AR defined as usual). The outer solution, valid for ε small, will be a lifting line for lifting bodies [1, 2], and a lifting line plus a line source for bluff bodies (Section 3). The inner coordinates are $Z = x_3, X = x_1/\varepsilon, Y = x_2/\varepsilon$, and the inner solution will be given by a free-streamline wake model which uses the complex variable $z = X + \mathrm{i}Y$ (Section 2). If the velocity potential in the outer solution is $\phi(x_1, x_2, x_3)$ then we have the relation $\Phi(X, Y, Z) = \varepsilon^{-1}\phi(x_1, x_2, x_3)$, where Φ is the velocity potential for the inner solution in the Z-section [2].

2. Inner solution

The two-dimensional inner solution in the Z-section is a modified version of the Tulin double spiral vortex model [7] which we have introduced in [8]. The relevant flow quantities are given in terms of a complex parameter x which varies over the upper half of an auxiliary plane. The polygonal obstacle section corresponds to $-1 \leqslant x \leqslant 1$, the spiral vortices to $x_S \in (1, \infty)$, $x_{S'} \in (-\infty, -1)$, and the points $x = \infty$ and $z = \infty$ correspond. The vertices of the polygon are denoted by $\{\hat{x}_k\}$, $\hat{x}_k \in \mathbb{R}$, $\zeta(x)$ is the complex velocity, w the complex potential, $\mathrm{d}w/\mathrm{d}z = \zeta$, and $\omega = \ln(\zeta)$. We have then, keeping the same notations as in [8]:

$$w(x) = (x - x_*)^2 W/2, \quad \mathrm{d}z/\mathrm{d}x = W[\zeta(x)]^{-1}(x - x_*) \equiv W\mathrm{e}^{-\omega(x)}(x - x_*) \tag{1}$$

where W is a positive constant (or order ε) and x_* is the parameter corresponding to the stagnation point on the obstacle. If the near-wake free-streamline speed $q_1 = (1 + \sigma)^{1/2}$ and x_S, $x_{S'}$, are fixed, the parameters $\{\hat{x}_k\}$, W are determined in terms of the side lengths of the polygon by solving the associated system of equations [8, 5]. Here the condition $\zeta(\infty) = 1$ must be replaced by $\zeta(\infty) = \exp(\mathrm{i}\alpha_D)$ (see Section 3) where α_D is the downwash angle, and this implies

$$x_* = -\cos\left\{\pi\hat{\gamma}_n + \alpha_D - \sum_{k=1}^{n-1}\beta_k \cos^{-1}(-\hat{x}_k) - \frac{1}{\pi}\ln(q_1)\ln\left[\frac{x_S + (x_S^2 - 1)^{1/2}}{|x_{S'}| + (x_{S'}^2 - 1)^{1/2}}\right]\right\} \tag{2}$$

where $\hat{\gamma}_k$ is the angle that the k-th side makes with the horizontal and $\beta_k = \hat{\gamma}_{k+1} - \hat{\gamma}_k$. (It should be remembered that all of these parameters depend on Z). Formula (2) replaces equation (9) of [8].

From equations (2)–(11) of [8] we find that the asymptotic expansion

$$\omega(x) = \omega_0 + \omega_1 x^{-1} + \omega_2 x^{-2} + \mathrm{O}(x^{-3})$$

holds as $x \to \infty$, where $\omega_0 = \mathrm{i}\alpha_D$, ω_1 and ω_2 are purely imaginary quantities given below. If we integrate the expression for $\mathrm{d}z/\mathrm{d}x$ from x_*, we obtain

$$z = W\exp(-\mathrm{i}\alpha_D)\left[\tfrac{1}{2}x^2 - \omega_1^* x - (\omega_2^* - \tfrac{1}{2}\omega_1^2)\ln(x)\right] + \mathrm{O}(1)$$

where $\omega_1^* = \omega_1 + x_*$, $\omega_2^* = \omega_2 - \omega_1 x_*$. Since

$$x = (2w/W)^{1/2} + x_* = (2w/W)^{1/2} + \mathrm{O}(1),$$

we have

$$z = \exp(-\mathrm{i}\alpha_D)[w - \omega_1(2Ww)^{1/2} - \tfrac{1}{2}W(\omega_2^* - \tfrac{1}{2}\omega_1^2)\ln(w)] + \mathrm{O}(1). \tag{3}$$

Note that the treatment here is at variance with Furuya [2] because of the absence of a free surface (cf. Birkhoff and Zarantonello [9], p. 70). As we shall see this affects the matching in an essential way.

Inverting (3) yields

$$w = \exp(\mathrm{i}\alpha_D)z + [2W\exp(\mathrm{i}\alpha_D)]^{1/2}\omega_1 z^{1/2} + \tfrac{1}{2}W(\omega_2^* - \tfrac{1}{2}\omega_1^2)\ln(z) + \mathrm{O}(1)$$

as $z \to \infty$, where

$$\omega_1 = -\mathrm{i}\left\{(1 - x_*^2)^{1/2} + \sum_{k=1}^{n-1}\beta_k(1 - \hat{x}_k^2)^{1/2} - \frac{1}{\pi}\ln(q_1)\left[(x_S^2 - 1)^{1/2} + (x_{S'}^2 - 1)^{1/2}\right]\right\}, \tag{4}$$

$$\omega_2 = -\frac{\mathrm{i}}{2}\left\{x_*(1 - x_*^2)^{1/2} + \sum_{k=1}^{n-1}\beta_k\hat{x}_k(1 - \hat{x}_k^2)^{1/2} - \frac{1}{\pi}\ln(q_1)\left[x_S(x_S^2 - 1)^{1/2} + x_{S'}(x_{S'}^2 - 1)^{1/2}\right]\right\}, \tag{5}$$

and n ($n \geqslant 1$) is the number of sides of the polygon (this number may vary with Z, see case (III) of Section 5).

We obtain then the outer expansion of the inner solution

$$\begin{aligned}\Phi(X, Y, Z) &\equiv \mathrm{Re}[w(z)]|_{Z\text{-section}} \\ &= X\cos\alpha_D - Y\sin\alpha_D + \mathrm{Re}[Az^{1/2}] - \tfrac{1}{8}W\omega_1^2\ln(X^2 + Y^2) \\ &\quad + \frac{\mathrm{i}}{2}W\omega_2^*\tan^{-1}(Y/X),\end{aligned} \tag{6}$$

where $A = \omega_1[2W\exp(\mathrm{i}\alpha_D)]^{1/2}$ is complex and ω_1, ω_2^* are purely imaginary. Notice that $A = \mathrm{O}(\sqrt{\varepsilon})$ as $\varepsilon \to 0$.

3. Outer solution and matching

Formula (6) suggests that for a low drag, lifting body we can take $\omega_1 = 0$, hence $A = 0$, and an outer solution given by the lifting-line potential [1, 2]

$$\phi_v(x_1, x_2, x_3) = x_1 - \frac{\varepsilon}{4\pi}\int_{-1}^{1} d\xi \frac{d\gamma}{d\xi}\left\{\tan^{-1}\left(\frac{x_2}{x_3 - \xi}\right)\right.$$

$$\left. + \tan^{-1}\left(\frac{x_2}{x_1}\frac{[x_1^2 + x_2^2 + (x_3 - \xi)^2]^{1/2}}{x_3 - \xi}\right)\right\} \tag{7}$$

to second order in ε. The inner expansion of the outer solution then yields [1, 2]

$$\varepsilon^{-1}\phi_v(\varepsilon X, \varepsilon Y, Z) = X - \frac{1}{2\pi}\gamma(Z)\tan^{-1}(Y/X) - \frac{\varepsilon}{4\pi} Y \oint_{-1}^{1} \frac{d\phi}{d\xi}\frac{d\xi}{Z - \xi} \tag{8}$$

to first order in ε. (The last integral is given by a Cauchy principal value.)

Matching (6) and (8), with $\omega_1 = 0$, we get

$$\gamma(Z) = -i\pi W\omega_2^*, \tag{9}$$

$$\alpha_D(Z) = \frac{\varepsilon}{4\pi}\oint_{-1}^{1}\frac{d\gamma}{d\xi}\frac{d\xi}{Z - \xi}. \tag{10}$$

Notice that $\gamma = O(\varepsilon)$, $\alpha_D = O(\varepsilon^2)$ as $\varepsilon \to 0$.

Thus, taking $\omega_1 = 0$, we can accomplish the matching with an outer solution given by a lifting line with circulation $\gamma(x_3)$, as is appropriate for a lifting body.

For a bluff body we should have ω_1 non-zero. We need then an outer solution which matches (6) with $\omega_1 \neq 0$, so that (6) includes both the log and the square-root terms (cf. [9], p. 68 and ff., again). The log term can be accounted for by adding to (7) the potential of a line distribution of sources

$$\phi_s(x_1, x_2, x_3) = -\frac{\varepsilon^2}{4\pi}\int_{-1}^{1}[\varrho^2 + (x_3 - \xi)^2]^{-1/2}\mu(\xi)d\xi \tag{11}$$

with density $\mu(x_3)$ on $-1 \leqslant x_3 \leqslant 1$ ($\varrho = (x_1^2 + x_2^2)^{1/2}$). The inner expansion is

$$\varepsilon^{-1}\phi_s(\varepsilon X, \varepsilon Y, Z) = \frac{\varepsilon}{2\pi}\mu(Z)\ln(r) + f(Z, \varepsilon) \tag{12}$$

(to first order in ε), where $r = (X^2 + Y^2)^{1/2} \equiv \varrho/\varepsilon$, and (cf. [10], p. 234)

$$f(Z, \varepsilon) = \frac{\varepsilon}{4\pi}\int_{Z}^{1}\frac{d\mu}{d\xi}\ln\left[\frac{2}{\varepsilon}(\xi - Z)\right]d\xi - \frac{\varepsilon}{4\pi}\int_{-1}^{Z}\frac{d\mu}{d\xi}\ln\left[\frac{2}{\varepsilon}(Z - \xi)\right]d\xi$$

$(+ o(\varepsilon^2))$ does not depend on X, Y (moreover $f = o(1)$ as $\varepsilon \to 0$). Then matching the log term in (6) with (12) gives

$$\mu(Z) = -\frac{\pi}{2}[\omega_1^2 W/\varepsilon]|_Z. \tag{13}$$

(Note that $\omega_1^2 \leqslant 0$, hence $\mu(Z) \geqslant 0$; also $\mu = O(1)$ as $\varepsilon \to 0$).

It remains to match the term $\mathrm{Re}[Az^{1/2}]$. From the definition of A and (13) we find

$$\mathrm{Re}[Az^{1/2}] = -\frac{2}{\sqrt{\pi}}[\varepsilon r \mu(Z)]^{1/2} \sin\left[\tfrac{1}{2}(\alpha_D + \tan^{-1}(Y/X))\right] \tag{14}$$

where $\alpha_D = O(\varepsilon^2)$. This term can be matched with an outer potential given by the harmonic function

$$\phi_r(x_1, x_2, x_3) = -\sqrt{2}\,\varepsilon \sum_{k=0}^{\infty} a_k k^{-1/2} \cosh(kx_3) J_{1/2}(k\varrho) \sin(\theta/2) \tag{15}$$

where $\theta = \tan^{-1}(x_2/x_1)$, and the a_k's are coefficients of the expansion of $\sqrt{\mu(Z)}$ in a Dirichlet series,

$$\sqrt{\mu(Z)} = \sum_{k=0}^{\infty} a_k e^{-kZ}$$

(recall that μ is nonnegative and even). Convergence of this series is guaranteed by Müntz's theorem [11].

It is easy to verify that the inner expansion of (15) coincides to first order in ε with (14). Summarizing, the outer solution for a bluff body is given by

$$\phi = \phi_v + \phi_s + \phi_r. \tag{16}$$

The circulation $\gamma(Z)$ is related to the two-dimensional lift coefficient $C_L(Z) = L(Z)/[\frac{1}{2}\varrho_0 q_\infty^2 l(Z)]$, $L(Z)$ the lift on the Z-section, by

$$\gamma(Z) = \tfrac{1}{2} l(Z) C_L(Z). \tag{17}$$

We also assume, following [2], the condition

$$\gamma(Z) = \Phi(X_S, Y_S, Z) - \Phi(X_{S'}, Y_{S'}, Z)$$

which modifies the spiral vortex model.

Using the expression (1) for $w(x)$ and equation (9) we get

$$\tfrac{1}{2} W[(x_S - x_*)^2 - (x_{S'} - x_*)^2] = -i\pi W \omega_2^*. \tag{18}$$

We need now to relate $\mu(Z)$ to the drag, $D(Z)$, on the Z-section. We fix μ by the condition $D(Z) = \varepsilon\mu(Z)$, as suggested by consideration of two-dimensional flow past a Rankine body generated by a source in a uniform stream [12]. Then, if $C_D(Z) = D(Z)/[\frac{1}{2}\varrho_0 q_\infty^2 l(Z)]$ is the two-dimensional drag coefficient and $c(Z) = l(Z)/l(0)$ (the normalized chord in the case of a wing), we have

$$\mu(Z) = c(Z)C_D(Z). \tag{19}$$

Our final matching equation,

$$[c(Z)C_D(Z)]^{1/2} = [-\tfrac{1}{2}\pi\omega_1^2 W/\varepsilon]^{1/2} \tag{20}$$

is obtained from (13) and (19). (The positive sign for the square root is chosen in order to ensure that the free streamlines do not cross.)

For consistency we require the underpressure (coefficient)

$$\sigma = (p_\infty - p_w)/[\tfrac{1}{2}\varrho_0 q_\infty^2]$$

(p_w is the near-wake pressure and p_∞ the pressure at infinity) to be constant in the three-dimensional near wake. However, we take account of the presence of a transverse flow velocity on the front of the body

$$u_Z = \frac{\partial}{\partial Z}[\Phi_v + \Phi_s + \Phi_r]$$

induced by the outer potential (here $\Phi_v = \varepsilon^{-1}\phi_v(\varepsilon X, \varepsilon Y, Z)$, and so on). This induced velocity will influence the value of the two-dimensional underpressure in the Z-section. For $\varrho \equiv \varepsilon r = 0$ (that is on the body seen from the far-field) we find from (8)

$$\partial\Phi_v/\partial Z = -\frac{1}{2\pi}\,\mathrm{d}\gamma/\mathrm{d}Z \quad (\varepsilon r = 0).$$

Analogously, from (11),

$$\partial\Phi_s/\partial Z = \frac{\varepsilon}{2\pi} Z(1 - Z^2)^{-1}\mu(Z).$$

Finally (15) implies

$$\partial\Phi_r/\partial Z = -2\pi^{-1/2}(\varepsilon r)^{1/2} \sin(\theta/2) \sum_{k=0}^{\infty} k a_k \sinh(kZ) = 0$$

at $\varrho = 0$ (to first order in ε). Thus the induced transverse velocity on the body is

$$u_Z = -\frac{1}{2\pi}\,\mathrm{d}\gamma/\mathrm{d}Z + \frac{\varepsilon}{2\pi} Z(1 - Z^2)^{-1}\mu(Z). \tag{21}$$

Then on a Z-section the near-wake free streamline speed will be

$$q_1(Z) = [1 + \sigma - u_Z^2(Z)]^{1/2}. \tag{22}$$

If we combine the expressions (4), (5) for ω_1, ω_2 with equations (18) and (20) we obtain the (fixpoint) equations

$$x_S = \left[1 + \left\{\frac{\pi}{\ln(q_1(Z))}\left[(1 - x_*^2)^{1/2} + \sum_{k=1}^{n-1} \beta_k(1 - \hat{x}_k^2)^{1/2} - \left\{\frac{C_D(Z)l(Z)}{\pi W}\right\}^{1/2}\right] - (x_{S'}^2 - 1)^{1/2}\right\}^2\right]^{1/2} \tag{23}$$

and

$$x_{S'} = x_* - \left[(x_S - x_*)^2 - \pi x_*(1 - x_*^2)^{1/2} + \pi \sum_{k=1}^{n-1} \beta_k(\hat{x}_k - 2x_*)(1 - \hat{x}_k^2)^{1/2} + 2x_* \ln(q_1(Z))\{(x_S^2 - 1)^{1/2} + (x_{S'}^2 - 1)^{1/2}\} - \ln(q_1(Z))\{x_S(x_S^2 - 1)^{1/2} + x_{S'}(x_{S'}^2 - 1)^{1/2}\}\right]^{1/2} \tag{24}$$

for the parameters x_S, $x_{S'}$ on a Z-section, with x_* satisfying (2) with $q_1 = q_1(Z)$.

We remark that for a low-drag body ω_1 and μ approach zero (cf. equations (19), (20)) so that the outer solution (16) reduces to a lifting line. Also we see that ω_1^2 is proportional to $C_D(Z)$ and ω_2^* to $C_L(Z)$. Thus everything is consistent and we may take (16) as outer solution for all cases.

4. Iterations and discretization

The procedure for solving the problem can be summarized by the following scheme which involves an inner iteration ((iii) below) to determine the parameters for the inner two-dimensional flow and a outer iteration which determines the matching quantities $\gamma(Z)$ and $q_1(Z)$:

(i) Choose σ and the geometrical parameters.
(ii) Initialize $\alpha_D(Z) = 0$ and $q_1(Z) = (1 + \sigma)^{1/2}$.
(iii) Solve the two-dimensional (parameter) problem in Z-sections using previous values of $\alpha_D(Z)$ and $q_1(Z)$.
(iv) Compute $\gamma(Z)$ from (17) and $q_1(Z)$ from (22) (using (21) and (19)), hence $\alpha_D(Z)$ from (10).
(v) Repeat (iii) and (iv) until convergence is obtained.

The equations (23), (24) for x_S, $x_{S'}$ and the side lengths in (iii) are solved using the iteration procedure of [8]. This is done on a finite number of sections after discretization in Z as discussed below.

Following [2] it is convenient to approximate $\gamma(Z)$, $Z = -\cos\tilde{\theta}$, with the Fourier sine polynomial

$$\gamma(-\cos\tilde{\theta}) \cong \sum_{n=1}^{N} A_n \sin(n\tilde{\theta}), \quad 0 \leqslant \tilde{\theta} \leqslant \pi.$$

Since $\sin(n\tilde{\theta}) = \sin(\tilde{\theta})U_{n-1}(\cos\tilde{\theta})$, where U_{n-1} is the Tchebychev polynomial of the second kind, the Cauchy integral in (10) can be computed in closed form:

$$\alpha_D(Z) \cong \frac{\varepsilon}{4} \sum_{n=1}^{N} nA_n \frac{\sin(n\tilde{\theta})}{\sin(\tilde{\theta})}$$

(see [13], p. 785).

We consider sections corresponding to equally-spaced values of $\tilde{\theta}$ so that the discrete Z values are given by the Tchebychev nodes in $[-1, 1]$,

$$Z_j = -\cos(j\pi/N), \quad j = 1, \ldots, N-1.$$

The advantages of this are twofold: the nodes are denser near the ends, and the values of γ and the Fourier sine coefficients A_n are related by a discrete sine Fourier transform, so that FFT algorithms can be applied if the number of sections is large. In fact we have:

$$\gamma_j = \sum_{n=1}^{N-1} A_n \sin(nj\pi/N),$$

$$\alpha_j = \varepsilon[4\sin(j\pi/N)]^{-1} \sum_{n=1}^{N-1} nA_n \sin(nj\pi/N),$$

$$A_n = \frac{2}{N} \sum_{j=1}^{N-1} \gamma_j \sin(nj\pi/N),$$

where $j, n = 1, \ldots, N-1$, N even, and $\gamma_j = \gamma(Z_j)$, $\alpha_j = \alpha_D(Z_j)$.

This numerical procedure can be efficiently implemented on a parallel computer, as it happens in general with "strip methods" [10].

5. Numerical results

We have written a FORTRAN program to implement the iterations (ii)–(v) of the previous section. In the inner iteration (iii), for each Z_j, the parameters $W, \hat{x}_1, \ldots, \hat{x}_{n-1}$ are determined, for fixed $x_S, x_{S'}$, by the side lengths of the polygon as in [8], [5]. The determination of $x_S, x_{S'}$ from equations (23) and (24), which we may think of as

$$x_S = f(x_S, x_{S'}), \quad x_{S'} = g(x_S, x_{S'}),$$

is done by successive replacements with a relaxation parameter ω_r,

$$x_S = \omega_r f(x_S, x_{S'}) + (1 - \omega_r)x_S,$$

$$x_{S'} = \omega_r g(x_S, x_{S'}) + (1 - \omega_r)x_{S'}$$

where $0 < \omega_r < 2$. The determination of ω_r was done by experiment and depended in an essential way on the section profile (as in [8]). Convergence was usually obtained in at most three iterations.

A similar relaxation procedure was used to update the values of $\gamma(Z)$ and $q_1(Z)$ in the outer iteration. The convergence criterion was given in terms of the section lift and drag coefficients.

This code was applied to the prototype problems described below. The three-dimensional drag and lift coefficients are defined by

$$C_D = \int_{-1}^{1} \hat{c}(Z)C_D(Z)\mathrm{d}Z, \quad C_L = \int_{-1}^{1} \hat{c}(Z)C_L(Z)\mathrm{d}Z$$

where

$$\hat{c}(Z) = c(Z)\Big/\int_{-1}^{1} c(Z)\mathrm{d}Z, \quad c(Z) = l(Z)/l(0).$$

The numerical computations have been performed on the IBM 3081 at WSU in Wichita, and on the VAX 8200 in Rome. In all cases 25 sections were used: Figure 1 shows, in a typical case, that the results are stable when the number of sections varies in this range [22].

(I) Oblique flat-plate airfoil with separation at the leading edge (supercavitating hydrofoil)

This problem has been extensively treated in the literature and experimental data are also available. We restrict our attention here to rectangular plan forms, but we have considered more general forms, as e.g., elliptic foils (see Figs. 6, 8 below).

For small angles of attack α our results are in excellent agreement with the linearized theory of Widnall [14]. As an example, Figure 2 shows values of C_L versus σ for $\alpha = 10$ degrees and aspect ratio AR = 4: experimental data by Kermeen [15] (squares) and Schiebe and Wetzel [16] (black circles) are included.

For large values of α, our results are in reasonable agreement with those of Furuya [2]: there are discrepancies which we think may be due to the influence of the free surface on Furuya's results. As an example, Figure 3 gives C_L and C_D versus σ at angle of attack $\alpha = 16.5$ degrees and AR = 6: experimental data from [16] (black circles) and Furuya's solution (dashed line) are included for comparison.

For wings of elliptic planform, the downwash turns out to be constant along the span as it is for a fully wetted flow [1] (cf. Figs. 6, 8 below).

(II) Flow past a flat plate airfoil with jet separation from the upper surface

The corresponding two-dimensional flow has been treated in a classical paper by Chaplygin and Lavrent'ev (see [17]). It was shown there that if separation occurs at the trailing edge,

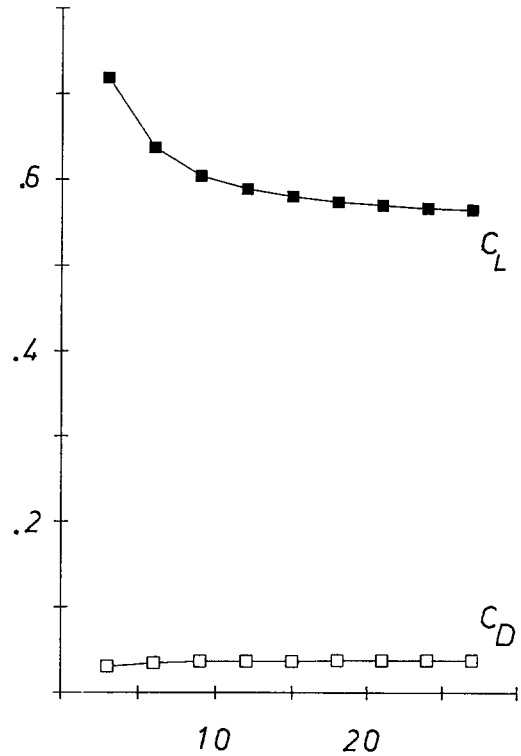

Fig. 1. Variation of C_L and C_D vs. number of sections for flat-plate wing of rectangular planform with partial spoiler at $\alpha = 10°$, $\delta = 60°$, AR = 6, $\sigma = 0.2$.

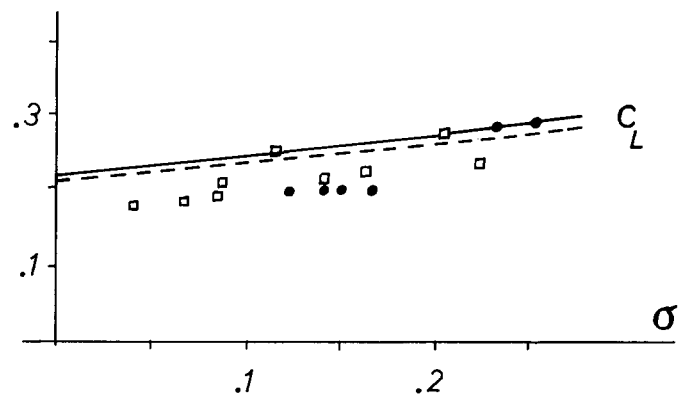

Fig. 2. Lift coefficient vs. underpressure σ for supercavitating hydrofoil (rectangular planform) at $\alpha = 10°$ and AR = 4.

as we assume here, the lift agrees with that of a fully wetted wing (with Kutta condition at the trailing edge).

We show in Table 1 the effect of aspect ratio on lift for rectangular and elliptic planform (together with the constant downwash for the elliptic wing) at $\alpha = 5$ degrees, $\sigma = 0$. Notice that the value $C_L = 0.55$ for a large aspect ratio agrees with the theoretical value $2\pi \sin \alpha$.

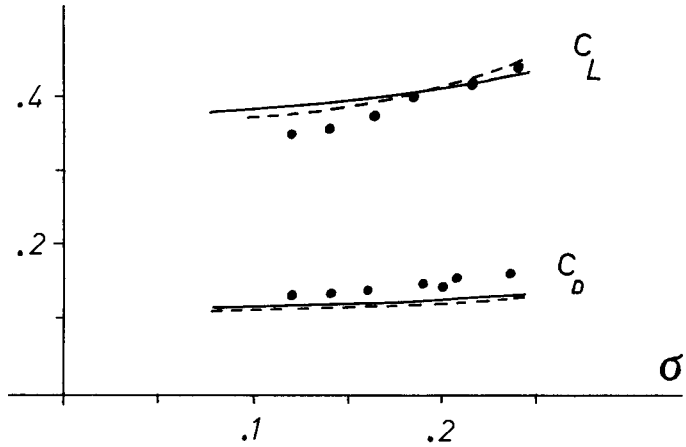

Fig. 3. Lift and drag coefficients vs. underpressure σ for supercavitating hydrofoil (rectangular planform) at $\alpha = 16.5°$, AR = 6.

Table 1.

AR	1000	20	15	10	6	4	
C_L	0.555	0.551	0.537	0.518	0.481	-	RECTANGULAR
C_L	0.555	0.553	0.552	0.550	0.522	0.478	ELLIPTIC
α_D	6.4×10^{-8}	1.6×10^{-2}	2.9×10^{-2}	6.4×10^{-2}	0.31	0.69	

(*III*) *Flat-plate wing (rectangular planform) with spoiler*

We consider a 10% spoiler at 77.5% chord with a range of deflection angles δ. Both 50% span spoiler ($-0.5 \leqslant Z \leqslant 0.5$) and a full span spoiler are reported at $\alpha = 10$ degrees, $\sigma = 0.2$, and AR = 20 and 6 (Table 2, δ in degrees). The results for aspect ratio AR = 20 (AR = ε^{-1}) are shown in Figure 4, for both partial (P) and full spoiler (F), and compared with the experimental data from [18] (squares). The figure gives incremental lift (changed of sign), $\Delta C_L = C_L(\delta) - C_L(0)$, versus spoiler deflection δ. In a linear approximation, this

Table 2.

Partial Spoiler			*Full Spoiler*		
δ	C_L	C_D	C_L	C_D	
5	1.13	0.0011	1.07	0.0015	
20	0.985	0.0043	0.685	0.0094	
40	0.836	0.0128	0.310	0.0290	
60	0.745	0.0210	0.070	0.050	AR = 20
80	0.695	0.027	−0.060	0.065	
120	0.693	0.028	−0.062	0.068	
5	1.05	0.012	0.946	0.0156	
20	0.905	0.015	0.608	0.0156	
40	0.763	.023	0.278	0.030	
60	0.671	.031	0.065	0.051	AR = 6
80	0.621	.038	−0.054	0.066	
120	0.618	.039	−0.058	0.069	

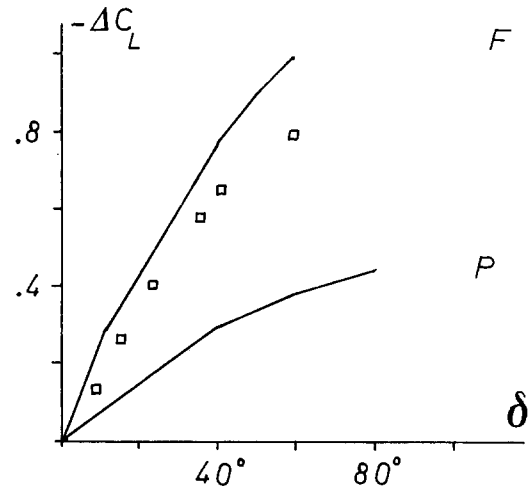

Fig. 4. Incremental lift vs. spoiler deflection δ for rectangular flat-plate wing with full and partial (50%) span spoiler.

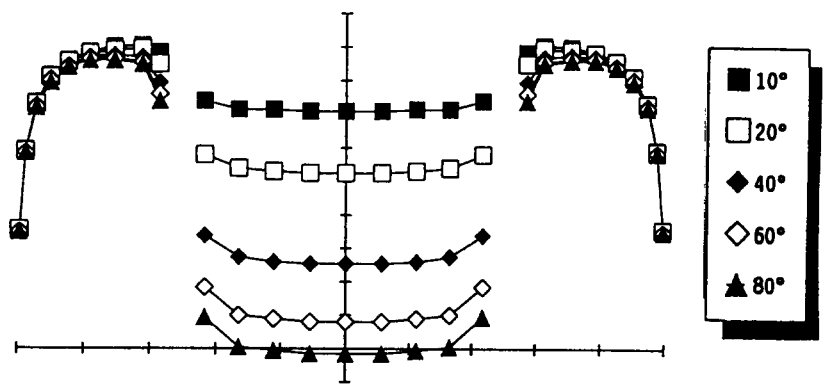

Fig. 5. Circulation $\gamma(Z)$ vs. span Z for a flat-plate wing of rectangular planform with partial (50%) span spoiler.

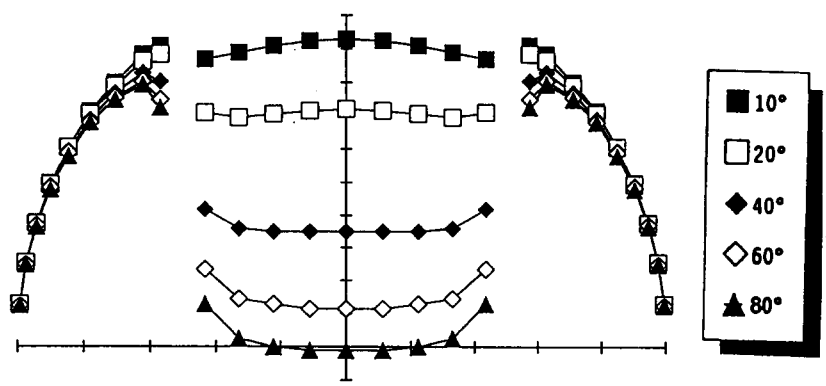

Fig. 6. Circulation γ vs. Z for a flat-plate wing of elliptic planform with partial spoiler.

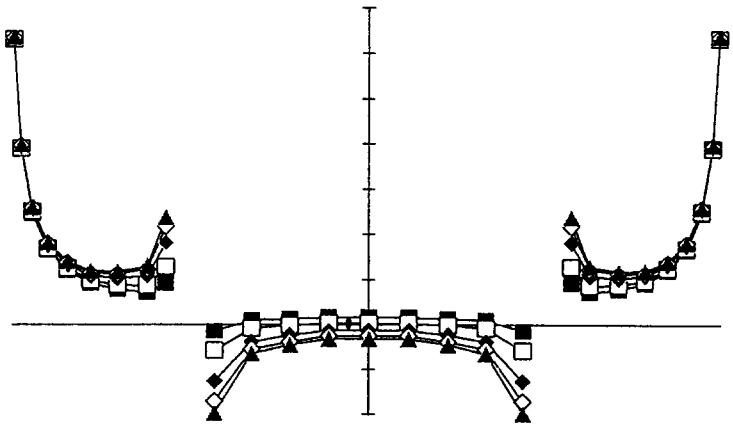

Fig. 7. Downwash angle vs. Z for a flat-plate wing of rectangular planform with partial spoiler.

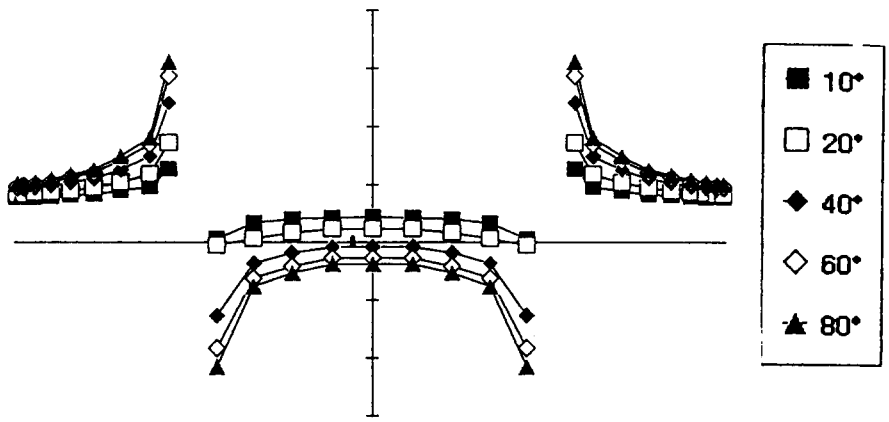

Fig. 8. Downwash α_D vs. Z for a flat-plate wing of elliptic planform with partial spoiler.

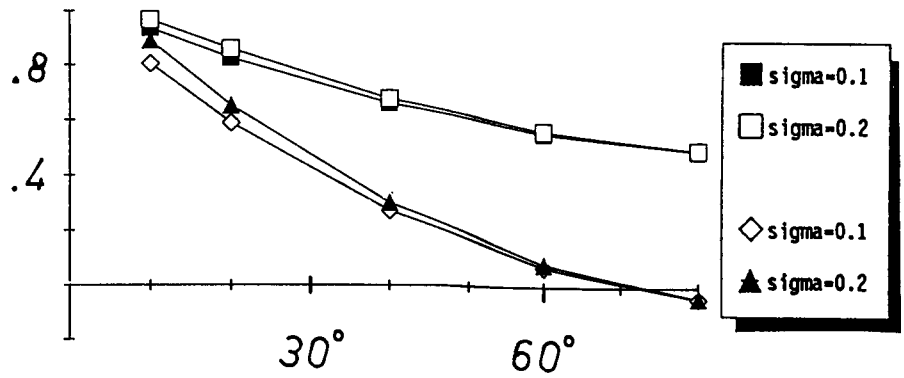

Fig. 9. Lift coefficient vs. spoiler deflection for a flat-plate wing with full and partial spoiler at $\alpha = 10°$, AR = 6, and $\sigma = 0.1, 0.2$.

quantity does not depend on thickness and camber of the foil (see [10]). The figure suggests a possible origin of the discrepancy between theoretical and observed data.

Figs. 5–9 concern a flat-plate wing with partial spoiler ($-0.5 \leqslant Z \leqslant 0.5$) with values $\alpha = 10°$, AR = 6, $\sigma = 0.2$, and a range of spoiler deflection angles from $\delta = 10°$ to $\delta = 80°$. Figure 5 shows the circulation $\gamma(Z)$ vs. Z for a wing of rectangular planform, and Figure 6 the circulation $\gamma(Z)$ for a wing of elliptic planform. The corresponding downwash is given in Fig. 7 for rectangular and Fig. 8 for elliptic planform. Finally, Fig. 9 shows C_L vs. δ for both partial spoiler (top curves) and full spoiler (bottom) at $\sigma = 0.1$ and 0.2.

(IV) GA(W)-2 airfoil with partial spoiler

We consider here a wing with rectangular planform and a polygonal approximation (with 20 sides) of the GA(W)-2 section with a 10% spoiler at 77.5% chord and 50% span, at angle of attack $\alpha = 10°$, AR = 6 and $\sigma = 0.2$.

Table 3 gives results for C_L, C_D and $C_L(Z)$, $\alpha_D(Z)$ vs. Z for a few values of δ [22]. Here 10 sections are used. Corresponding values are plotted in Fig. 10. Agreement with experiments from [18] is found with discrepancies (due to neglection of viscosity) less than 20%.

(V) Orthogonal flat plate (rectangular plan-form)

The important feature to observe here is the variation of drag with aspect ratio: C_D should decrease with aspect ratio [19, 20]. Table 4 compares values of $C_D(\mathrm{AR})/C_D(\infty)$ as computed from our program (for $\sigma = 1$) with experimental data from [19, 20]. The poor agreement of our values with experiments is due to the fact that our outer solution does not include a significant inflow along the back of the plate (cf. [20]). The agreement can be improved with a correction factor which modifies q_1 on sections near the ends. For instance, taking $q_1(Z) = q_1(1)$ for sections having $0.75 \leqslant |Z| \leqslant 1$ gives a good agreement with experiment. It would be far more desirable to achieve this with an outer solution with inflow that can be consistently matched. This is an important unsolved problem to which we plan to return in future work.

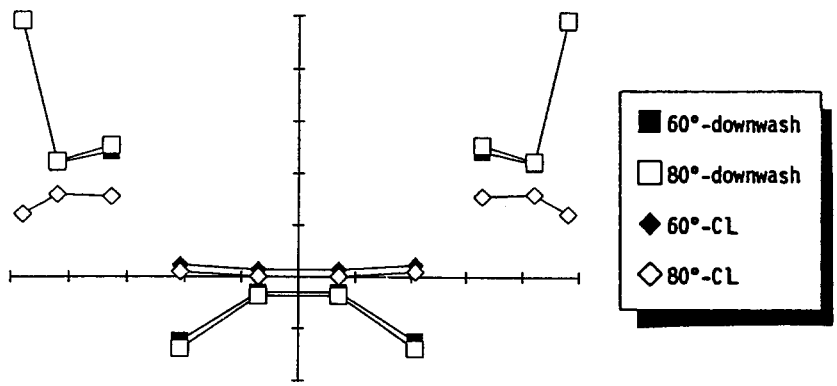

Fig. 10. 2D lift coefficient $C_L(Z)$ and downwash $\alpha_D(Z)$ vs. Z for a rectangular planform GA(W)-2 wing with partial spoiler at deflections $\delta = 60°$, 80° and $\alpha = 10°$, AR = 6, $\sigma = 0.2$.

Table 3.

δ	20°	40°	60°	80°
C_L	1.152	0.931	0.800	0.725
C_D	0.039	0.052	0.066	0.076

Z	α_D (δ = 60°)	α_Δ (δ = 80°)	$C_L(Z)$ (δ = 60°)	$C_L(Z)$ (δ = 80°)
−0.960	4.898	4.922	1.223	1.220
−0.841	2.200	2.236	1.605	1.600
−0.655	2.417	2.538	1.575	1.558
−0.500				
−0.415	−1.234	−1.390	0.232	0.102
−0.142	−0.304	−0.364	0.140	0.006
0.142	−0.304	−0.364	0.140	0.006
0.415	−1.234	−1.390	0.232	0.102
0.500				
0.655	2.417	2.538	1.575	1.558
0.841	2.200	2.236	1.605	1.600
0.960	4.898	4.922	1.223	1.220

Table 4.

AR	∞	18	8	4	1
Experiment	1	0.70	0.64	0.60	0.57
Theory	1	0.99	0.985	0.971	0.898

6. Determination of near-wake underpressure

A relation between σ and the Reynolds number

$$R = q_\infty l(0)/\nu$$

where ν is the kinematical viscosity of the real fluid whose behavior is approximated by the present inviscid model has been proposed by Tulin and Hsu [21] and extended in [8] to transitional flows. This relation holds for fixed points of separation, and for a flat plate orthogonal to the stream the parameters can be adjusted to give (see equation (12) of [8]):

$$R = \begin{cases} 750(1+\sigma)^2[C_D(\sigma)]^{-1}[0.4\sigma^{-2}(1+\sigma)^{3/2} - 1]^{-1}, & R \geqslant R_S(\sigma) \\ 80(1+\sigma)[C_D(\sigma)]^{-1}\sigma^{-2}(1+\sigma)^{5/2}, & R \leqslant R_S(\sigma) \end{cases} \tag{25}$$

where

$$R_S(\sigma) = 3120(1+\sigma)^{1/2}\sigma^2[C_D(\sigma)]^{-1}$$

and $C_D(\sigma)$ is computed on the $Z = 0$ section. This relation can be inverted to give $\sigma = \sigma(R)$, a one-valued function [8]. Therefore the free parameter of the present theory can be chosen to be R. Relation (25) shows that for high Reynolds numbers, above a threshold value R_t, σ remains practically constant, so that C_L, C_D, . . . are insensitive to variations of R above this threshold. This agrees with experimental data for flows past obstacles with fixed points

of separation [19], and justifies the use of an inviscid wake model. For instance the experimental results of Table 4 were found for a range of values of R around 10^5, well above the threshold, where σ can be estimated to be around unity from the above (the denominator in the first equation (25) approaches zero).

Acknowledgment

This research was partially supported by Consiglio Nazionale delle Ricerche (C.N.R.) under contracts N. 86.02073.01 and N. 87.01011.01. The work of the first author was partially supported by Ministero Pubblica Instruzione (Fondi 40%) and by G.N.F.M. of C.N.R.. The work of the second author was supported in part by U.S. Air Force Grant AFOSR-86-0274. Thanks are due to Dr Ing. A. Mannini of Spectrum Corp. (Latina, Italy) for his interest in this work.

References

1. M. Van Dyke, *Perturbation Methods in Fluid Mechanics*, 2nd edn., Stanford, Parabolic Press (1975).
2. O. Furuya, Three-dimensional theory on supercavitating hydrofoils near a free surface, *J. Fluid Mech.* 71 (1975) 339–359.
3. P.D. Sclavounos, An unsteady lifting-line theory, *J. of Engineering Mathematics* 21 (1987) 201–226.
4. A.R. Ahmadi and S.E. Widnall, Unsteady lifting-line theory as a singular perturbation problem, *J. Fluid Mech.* 153 (1985) 59–81.
5. A.R. Elcrat and L.N. Trefethen, Classical free-streamline flow over a polygonal obstacle, *J. Comput. Appl. Math.* 14 (1986) 251–265.
6. R.L. Street, A review of numerical methods for solution of three dimensional cavity flow problems. In: Proc. 2nd Intern. Confer. on *Numerical Ship Hydrodynamics*, Univ. of California, Berkeley (Sept. 1977) 237–268.
7. M.P. Tulin, Supercavitating flows – small perturbation theory, *J. Ship Research* 7 (1964) 16–37.
8. P. Bassanini and A.R. Elcrat, A univalent spiral-vortex model for separated flow past a polygonal obstacle, *ZAMP* 39 (1988) 455–467.
9. G. Birkhoff and E.H. Zarantonello, *Jets, Wakes, and Cavities*, New York, Academic Press (1957).
10. J.N. Newman, *Marine Hydrodynamics*, Cambridge (Mass.), MIT Press (1978).
11. L. Schwartz, *Etude des Sommes d'Exponentielles Réelles*, Paris, Hermann & Co. (1943).
12. L.M. Milne-Thomson, *Theoretical Hydrodynamics*, London, MacMillan (1968).
13. M. Abramowitz and I.A. Stegun, *Handbook of Mathematical Functions*, New York, Dover (1965).
14. S.E. Widnall, Unsteady loads on supercavitating hydrofoils of finite span, *J. Ship Research* 10 (1966) 107–118.
15. T. Nishiyama, Lifting line theory of supercavitating hydrofoil of finite span, *ZAMM* 50 (1970) 645–653.
16. F.R. Schiebe and J.M. Wetzel, Ventilated cavities on submerged three-dimensional hydrofoils, *St. Anthony Falls Hydraulic Lab.*, University of Minneapolis, Tech. Paper, B36 (1961).
17. M.I. Gurevich, *Theory of Jets in an Ideal Fluid*, New York, Academic Press (1965).
18. W.H. Wentz, Wind tunnel tests of the GA(W)-2 airfoil with 20% aileron, 25% slotted flap, 30% Fowler flap and 10% slop-lip spoiler, NASA CR-145139 (1977).
19. S. Goldstein, *Modern Developments in Fluid Dynamics*, New York, Dover (1965).
20. S.F. Hoerner, *Fluid-Dynamic Drag*, Hoerner Fluid Dynamics, 7528 Stanton Place, NW., Albuquerque, N.M. 87120, USA (1986).
21. M.P. Tulin and C.C. Hsu, New applications of cavity flow theory, Proc. ONR Symposium on *Naval Hydrodynamics*, Tokyo (1980), National Academy Press, pp. 107–130.
22. S. Allione, Master's Thesis, Dept. of Mathematics, Univ. of Rome, Italy (Oct. 1988).